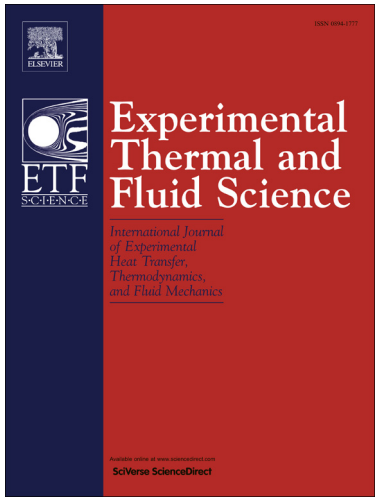

Film Thickness Measurement in Oil-Water Pipe Flow using Image Processing Technique

Adriana Bonilla Riaño, Iara H. Rodriguez, Antonio C. Bannwart, Oscar M.H. Rodriguez

PII: S0894-1777(15)00140-5
DOI: http://dx.doi.org/10.1016/j.expthermflusci.2015.05.004
Reference: ETF 8479

To appear in: *Experimental Thermal and Fluid Science*

Received Date: 20 March 2015
Revised Date: 15 May 2015
Accepted Date: 18 May 2015

Please cite this article as: A.B. Riaño, I.H. Rodriguez, A.C. Bannwart, O.M.H. Rodriguez, Film Thickness Measurement in Oil-Water Pipe Flow using Image Processing Technique, *Experimental Thermal and Fluid Science* (2015), doi: http://dx.doi.org/10.1016/j.expthermflusci.2015.05.004

Film Thickness Measurement in Oil-Water Pipe Flow using Image Processing Technique

Adriana Bonilla Riaño[a,*], Iara H. Rodriguez [b], Antonio C. Bannwart [a], Oscar M.H. Rodriguez [b]

[a] Department of Petroleum Engineering, University of Campinas (UNICAMP), Av. Mendeleyev 200, 13083-860, Campinas, SP, Brazil

[b] Department of Mechanical Engineering, São Carlos School of Engineering, University of São Paulo (USP), Av. Trabalhador São Carlense 400, 13566-570, São Carlos, SP, Brazil

[*] Corresponding author. Address: Av. Trabalhador São Carlense 400, 13566-570, São Carlos, SP, Brazil. Tel.: +55 1633738229. E-mail: adriana@dep.fem.unicamp.br

Abstract

Dispersed oil-water flow was studied in a 12 m long horizontal acrylic pipe, with 26 mm of internal diameter, using mineral oil (828 kg/m^3 of density and 220 mPa s of viscosity) and tap water. Experiments with a high-speed video camera were performed to obtain images of the flow near the pipe wall in highly dispersed oil-water flow. A visualization section was properly designed and installed in the pipeline for that purpose. The technique applied in the present work is based on the acquisition of images of the flow, and then the application of digital image processing techniques in order to quantify the film thickness near the wall. A thin water film was detected at the top and bottom of the pipe at highly turbulent oil-water flow. A pre-processing enhancement algorithm and a combined segmentation algorithm are being proposed to measure the film thickness. A comparison with a phenomenological model is also presented. The combined method performs better when compared with the results obtained from the application of the traditional techniques individually.

Keywords: Dispersed Oil-water Flow, Two-phase Flow, Water-film Thickness, Image Processing, Image improvement, Image Segmentation.

1 INTRODUCTION

The dispersed oil-water flow pattern, where the oil is dispersed as droplets into the water, is common in crude oil transportation, offshore wells and pipelines. However, it has not received as much attention as separated or intermittent flows. An interesting feature of this flow pattern is the drag reduction phenomenon, yet not well understood. The drag reduction phenomenon can be defined as a reduction in two-phase pressure gradient when compared to equivalent single-phase flow values. The occurrence of the drag reduction phenomenon without the addition of drag reduction agents in dispersed flow has been reported in some works [1]–[5]. For instance, Rodriguez et al. [6] observed a reduction of up to 25% of two-phase pressure gradient with respect to the corresponding single-phase water pressure gradient at the same mixture velocity in a viscous oil-water dispersed flow in a glass pipe. A phenomenological model that assumes the existence of a thin water film adjacent to the pipe wall was proposed to explain the drag-reduction mechanism, but it lacks experimental confirmation. Given the frequent occurrence of dispersed oil-water flows, the goal of this study is to investigate experimentally this flow pattern to further understand it and contribute to the modeling of hydrodynamic phenomena as the drag reduction.

Liquid films in two-phase flow are usually less than a few millimeters, so accurate measurement is difficult, which has led to the development of a wide range of measurement techniques [7]. Each technique has its own range of applicability, advantages, disadvantages and

limitations. As a rule, methods are developed having in mind specific experimental conditions and they are not suitable as general methods [8].

Several measurement techniques have been developed for the investigation of multiphase flows. Moreover, the existing literature covers mainly the application of these techniques in gas-liquid flows. Some film-thickness measurement techniques applied to liquid-liquid-flow investigation are photographic, capacitive probes and capacitive Wire-Mesh Tomography (WMT).

In [9] a photographic method is used to obtain water film thickness in core-annular flow. Wavelengths were seen to vary from 6 mm to 60 mm, while wave amplitudes were of the order of 1-2 mm. Authors mentioned the problem of optical distortion due to diffraction. A disadvantage of this method is that the measurements are only taken in a given area, i.e. in front of the camera (top and bottom for horizontal pipe, right and left for vertical pipe).

Capacitive sensors have been widely applied in the area of flows in pipes. These sensors are normally simpler, have fast response, non-intrusive and non-invasive nature, and flexibility in electronics design. Capacitive planar sensors can be used to investigate near-wall flows of nonconductive liquids. They make use of the relationship between electrical capacitance and film thickness. For example, Thiele et al [10] presented a capacitive planar sensor to visualize flows of multiphase mixtures along the surface of objects. The sensor comprises a matrix of 1024 interdigital sensing structures which are individually interrogated based on the capacitance wire-mesh sensor electronics [11]. The maximum liquid thickness, which influences the measurements at a sensor, is 750 µm. No application of this method in pipelines was found.

The wire-mesh sensor combines intrusive local measurement of phase fraction and tomographic cross-sectional imaging. The wire-mesh sensor based on measurements of electrical permittivity (capacitance) allows studying flows involving non-conducting fluids, such as oil-air flow. In [12] a wire-mesh based on capacitance was proposed to investigate a falling liquid film in gas-liquid flows. In that work, the local gas void fraction distribution was assumed to have a linear relationship with the measured permittivity and by using a geometrical ratio the liquid film thickness was found. The measured film thickness varies from 1.8 mm to 6.2 mm.

High frequency impedance probes have been used for local phase fraction measurements in low viscosity oil-water flows [13]. However, in order to measure the water film thickness in a dispersed viscous oil-water flow one would need a probe that would not be affected by oil. The viscous oil could stick to the conductive prove, compromising the data quality. For this kind of measurement, a capacitive technique would be more suitable as even with some amount of oil sticking to the probe surface it would still work. A paper recently published [14] describes a new planar capacitive probe that has been used for water film measurements. We have plans to compare that technique to the optical one described in the present paper.

In the present work, images of a highly dispersed oil-water flow were obtained with a high-speed video camera in an acrylic pipe with 26 mm of internal diameter and then processed. The aim of the experimental work was to confirm the existence of a water film and measure it. The first stage of that task was to improve the images, because they had noise and low contrast, which made the image processing difficult. Afterwards, image segmentation was applied to segregate oil regions from water regions.

The experimental setup and methods are presented. Thereafter, the image processing algorithm used to obtain the film thickness is described. The results and comparisons between experimental data and model predictions are presented. Finally, the main conclusions are summarized.

2 MATERIALS AND METHODS

2.1 Experimental setup

Experiments were performed with a high-speed video camera in the Multiphase-Flow rig of

LETeF (Thermal-Fluids Engineering Laboratory) at São Carlos School of Engineering - University of São Paulo. A camera Olympus *i*-speed3 was installed at 10.3 m from the entrance of a horizontal 12-m-long transparent acrylic pipe with 26 mm of internal diameter. The multiphase-flow loop is shown schematically in Figure 1 and the main instruments of the facility are listed in TABLE I.

Tap water and oil (828 kg/m^3 of density and 220 mPa s of viscosity) were used as test fluids. Water and oil are displaced from their respective storage tanks to the test line through their own series of pipes and positive displacement pumps. The two liquids join at the beginning of the test section via a Y-junction. Positive displacement flow meters were used to measure high and low oil flow rates and positive displacement and vortex flow meters were used to measure high and low water flow rates. After the test section the oil-water mixture flows to a 0.22 m^3 separator tank with coalescent-plates, where the fluids are separated by gravity. Finally, the oil and water phases return to their respective storage tanks. A computer was used to control the tests and to collect the data.

In this study measurements were made for mixture superficial velocities varying from 3.1 to 4.2 m/s and input oil fractions from 0.14 to 0.43, in total 12 experimental points.

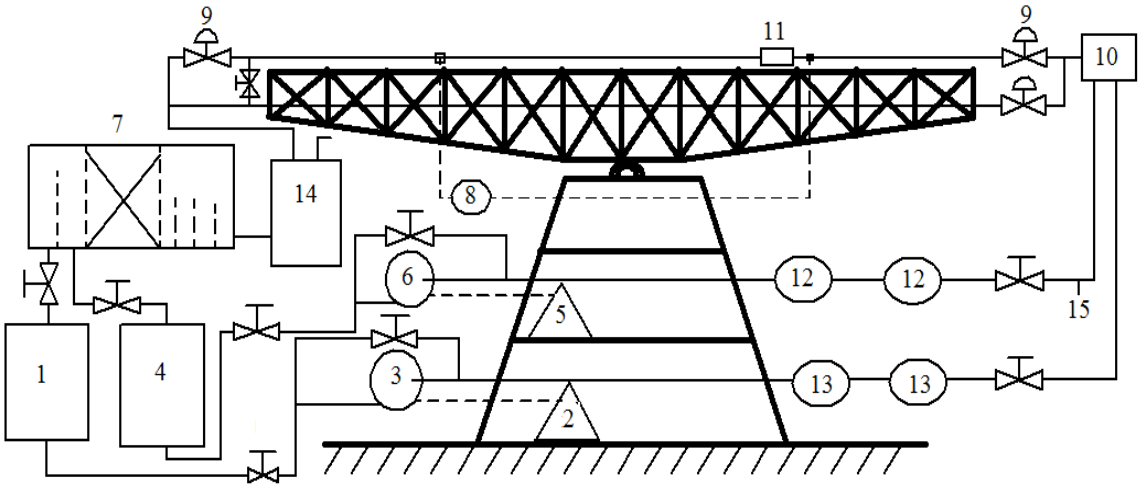

Figure 1. Schematic view of the multiphase flow loop at LETeF**.**

TABLE I Main instruments and equipment of the LETeF facilities.

Number	Element	Number	Element	Number	Element
1	Water Tank	7	Coalescent-Plates Liquid-Liquid Separator	13	Oil Flow Rate Meters
2	Water Variable-Frequency Driver	8	Differential Pressure Transducer	14	Gas-Liquid Separator Tank
3	Water Pump	9	Quick-Closing Valves	15	Temperature meter
4	Oil Tank	10	Multiphase Mixer		
5	Oil Variable-Frequency Driver	11	Visualization Section		
6	Oil Pump	12	Water Flow Rate Meters		

2.2 Flow visualization setup

The first challenge was to correct the optical distortions (parallax and lens effects) due to the pipe wall. There are several methods for correcting, minimizing or preventing optical distortion caused

by pipe curvature [15]–[18]. Some tests were carried out using a transparent box filled with fluids with different refractive indexes, but close to that of pipe material. Another attempt was made by using a solid acrylic box designed and constructed as an independent piece and then installed in the horizontal pipeline (Figure 2a). The latter showed the best results.

The next stage was to select a pattern length to insert into the visualization section for image calibration. A 0.2 mm×0.2 mm square pattern length was chosen after preliminary tests (Figure 2c). The square pattern was attached to a piece of acrylic and placed within the acrylic box in the center of the tube and perpendicular to the camera view (Figure 2b). Another acrylic box constructed with the same dimensions of the previous one was used for the flow visualization (Figure 3). It is important to note that the flow is recorded upstream of the pattern length, as shown in Figure 3, with the mixture flowing from right to left. This configuration ensures that the pattern does not disturb the flow.

For the lighting system, two LED lamps of 30W and 2300 lumen were used. Preliminary lighting tests were also made in order to find the best configuration/position of the lamps to obtain sharper images and a good contrast between the phases, oil and water. The lighting arrangement that presented best results was the one with the lamps positioned at the back and the bottom of the section (Figure 2a). In addition, a halogen lamp was located above the visualization section during the tests. An AF-S Micro Nikkor 60 mm f/2.8D lens was used for recording the images at a frame rate of 5000 frames/s.

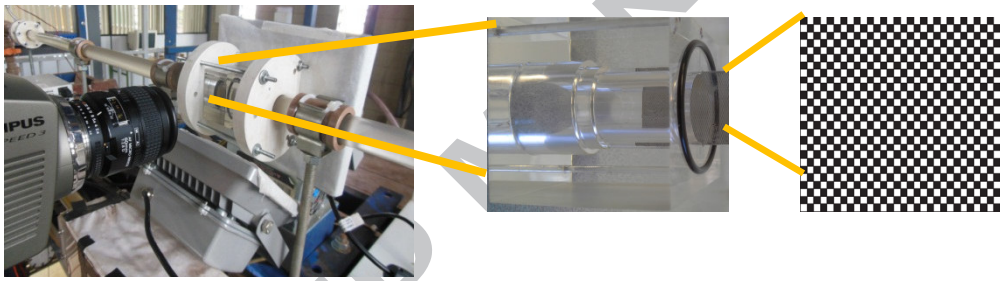

(a) (b) (c)

Figure 2. (a) Camera setup; (b) Side view of the acrylic box with the square pattern length attached; (c) Square pattern length used for image calibration (0.2 mm×0.2 mm).

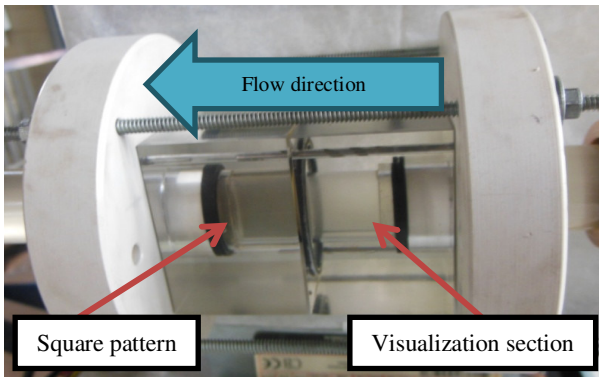

Figure 3. Entire visualization section

2.3 Experimental procedure

The experimental procedure had the following steps:

1- The pipe is first filled with water and an image of the pattern is recorded (Figure 4).
2- Experiments begin with single-phase water flow. After some time, oil is gradually added. After reaching steady state, the high-speed camera is activated and the two-phase oil-water

flow is recorded. Figure 5 shows snapshots of flows of mixtures with different oil and water superficial velocities, U_{os} and U_{ws}, respectively. It is possible to observe narrow strips near the pipe wall clearly dominated by water at the top and bottom of the pipe. In Figure 5, the red boxes are the regions of interest used for the film thickness measurements. The observed water-film region is not a region completely free from drops. An oil drop may eventually be seen near the pipe wall, but it was always repelled towards the dispersed core. We are adopting the assumption that there is a statistically stable water film, with a characteristic space and time averaged thickness.

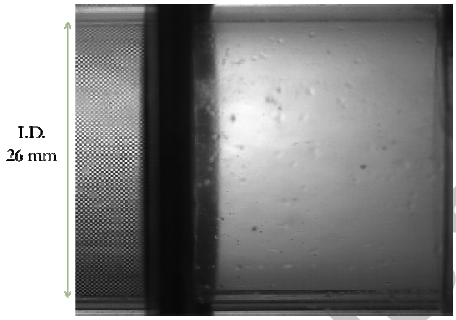

Figure 4. Square pattern length and visualization section with the pipe filled with water.

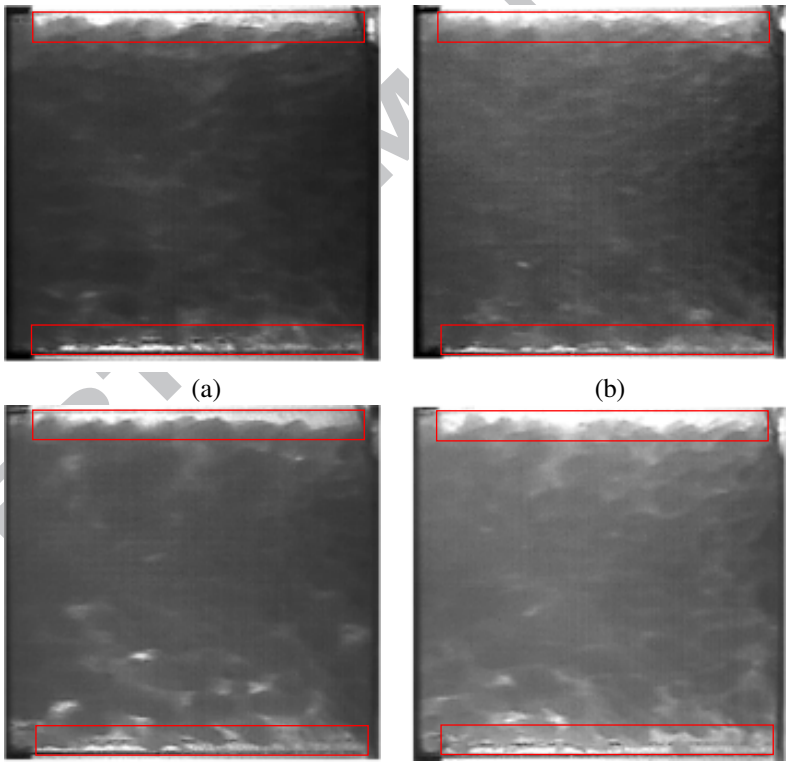

Figure 5. Images of the dispersed oil in water dispersed flow pattern: (a) U_{ws}=2.5 m/s, U_{os}=1.2 m/s; (b) U_{ws}=2.5 m/s, U_{os}=1.5 m/s; (c) U_{ws}=2.0 m/s, U_{os}=1.1 m/s; (d) U_{ws}=2.0 m/s; U_{os}=1.2 m/s. Red boxes are the regions of interest used to film thickness measurements.

3- The last step consists in data treatment or processing the images for quantification of water film thickness at the top and bottom of the pipe, respectively.

3 IMAGE PROCESSING

An automatic image-processing algorithm is proposed in Figure 6. The algorithm includes pre-processing, segmentation and film thickness estimation. The pre-processing includes cutting, improving and calibrating the image. In the segmentation stage it is important to select a suitable method to manipulate such images, for instance in [19] two segmentation methods were tested for oil-water core-annular flow image analysis. Finally, the average water film thickness is calculated in the film thickness estimation stage.

Figure 6. Proposed algorithm for the film thickness calculation.

3.1 Pre-processing

The images of the dispersed oil-water flow would have noise and low contrast. Therefore, pre-processing was needed to improve the images for better data interpretation. Some popular techniques or methods for improving image quality are: contrast improvement, edge enhancement (e.g. deblurring), spatial (e.g. averaging, median, adaptive filters) and frequency filtering techniques (Fourier and Wavelet domain). Different methods for image enhancement have been compared in [20]. The performance of those methods was evaluated using predefined image quality metrics or parameters, as Mean Squared Error, Mean Average Error, Peak Signal to Noise Ratio, among others. The techniques that provided better results were Contrast Limited Adaptive Histogram Equalization (CLAHE) with Rayleigh distribution, Wavelet denoising and Unsharp filter.

The possible combinations of these methods were implemented and compared in order to assess the best sequence to be applied for improving the images quality. The most favorable option was applying the methods in the following sequence: Wavelet denoising, Unsharp filtering and CLAHE with Rayleigh distribution. The proposed combination sequence showed the lowest values of error. Moreover, a better visual image was achieved by using a combination of methods instead of using a single method.

The method Contrast Limited Adaptive Histogram Equalization (CLAHE) computes several histograms, each corresponding to a distinct region of the image, and applies the histogram equalization to each one with a defined distribution. The objective of the process is to improve the local contrast of an image.

The method uses a limit parameter value of the histogram in order to obtain adequate brightness and contrast on the enhanced image. The contrast limit is controlled on the histogram equalization process. A criterion for the desired histogram distribution is defined based on the contrast range of the original image. The criterion for histogram distribution is either uniform, exponential, or Rayleigh. Therefore, the natural properties of the original image can be maintained since the distribution form is not significantly changed after enhancement process [21].

Wavelet denoising method relies on the fact that noise commonly manifests itself as fine-grained structure in the image. Consequently, most of the noise tends to be represented by wavelet coefficients at the finest scales. Eliminating these coefficients would result in a natural filtering of the noise. There are some variables of the wavelet denoising method of images to be studied: the wavelet function and the level N of wavelet decomposition, the wavelet thresholding function and the threshold itself [22].

Wavelet denoising consists of three main stages:

- Perform a discrete wavelet transform (DWT) to the noisy image.
- Application of threshold, in order to suppress coefficients due to noise.

- Reconstruct the denoised image by applying the inverse discrete wavelet transform (IDWT) on the processed highpass wavelet subimages to obtain an estimate of the noise-free image.

Denoising reduces the noise level but the resultant image could be blurred or over smoothed due to losses like edges or lines. Unsharp filter was selected to deblurring the images after the denoising step. The Unsharp filter enhances edges (and other high frequency components in an image) via a procedure which subtracts an unsharp or smoothed version of an image from the original image [23].

3.2 Segmentation

Segmentation is the separation of digital images in multiple regions that are homogeneous with respect to one or more attributes [23]. For the pre-processed dispersed oil-water flow images, it is assumed that there are two different classes: oil and water.

3.2.1 Segmentation by Thresholding

Thresholding is the most basic pixel-based segmentation. The application of this method results in a binary image with different objects. Depending on the application, objects are represented by a gray level 0 (white) and the background is represented as 1 (black) or vice versa.

One way to remove objects to the background is to choose a threshold T. Thus, any point (x,y) for which $f(x,y)>T$ is called object, in the opposite case the point is called background [24].

There are many algorithms to calculate the threshold. The first one used in this work was Otsu´s algorithm, which is one of the classical methods. The pixels of the image are divided into two classes, C_1 with gray levels [0 to T] and C_2 with gray levels [$T+1$ to $L-1$]. The Otsu method chooses the optimal threshold T by minimizing the intra-class variance [25], [26].

The second one is the ISODATA algorithm, which is an iterative algorithm. In general, it assigns an arbitrary initial value of threshold. The second step classifies each pixel to the closest class. In the third step the mean values (μ_1 and μ_2) of each class are estimated using Gaussian distribution. In the next step it is calculated a new threshold as $\mu_1+\mu_2/2$. The second and third steps are repeated until the change between the iteration is small enough [27], [28].

The last one is fuzzy partition and Tsallis entropy based thresholding [29]. In this case, the image is divided into different classes by selecting multiple threshold points by performing fuzzy partition on a 2D histogram based on fuzzy relation and maximum fuzzy entropy principle. The entire distribution is divided into n classes, and the Tsallis entropy, H_n^α, for each distribution is determined as

$$H_n^\alpha = \frac{1}{\alpha-1}\left[1-\sum_{g=0}^{L-1}\left(\frac{p(g)M_n}{w_n}\right)^\alpha\right], \qquad (1)$$

where L is the number of gray levels in the image, α is a real positive parameter not equal to one, $p(g)$ is the probability of occurrence of a gray level g in the image, w_n is the gray level probability distributions for the n class and M_n is the fuzzy membership function.

The optimum value of parameters can be obtained by maximizing the total entropy as

$$\varphi = Arg\max\left(\left[H_1^\alpha + H_2^\alpha + ... + H_n^\alpha + (1-\alpha)H_1^\alpha H_2^\alpha ... H_n^\alpha\right]\right). \qquad (2)$$

3.2.2 Mathematical morphology

Mathematical morphology is a non-linear image processing technique. Morphology operates on image regions that can be reshaped under the control of a structuring element. It is composed of two basic operators: erosion and dilatation. Other operators can be defined based in these two basic operations, for example opening and closing. Morphological erosion operation erodes away the boundaries of regions. As a result areas of foreground pixels shrink in size, and holes within those areas become larger. Morphological dilation operation gradually enlarges the boundaries of regions.

Areas of foreground pixels grow in size while holes within those regions become smaller. On the other hand, opening and closing operations are known to isolate structures that are brighter and darker than their surroundings, respectively [30].

3.2.3 Wavelet Transform

The main feature of the wavelet transform for segmentation is that it is capable of representing a signal in the spectral and temporal domain simultaneously [36]. The pixels features are extracted after the Wavelet transform, i.e. forming for each original pixel a feature vector. This feature vector is composed by the original gray value and five intensities from sub-images approximation coefficients at the same coordinate.

For classification, self-organizing neural networks were used in [31], but k-means or any other unsupervised learning algorithm could be used. In our work, fuzzy c-means and k-means [32] algorithms were used.

3.2.4 Proposed combined method

A combined method for dispersed oil-water flow image segmentation is proposed in this work. The segmentation algorithm includes: wavelet decomposition, fuzzy partition and Tsallis entropy based thresholding with three thresholds (each pixel on the image is approximated to one of this thresholds), conversion to binary using the histogram and morphological opening (to fill small holes). The flowchart of the combined algorithm and the results for each step are shown in Figure 7. The processed images correspond to the top and bottom section of the pipe (Figure 5). A snapshot of an image of the water film at the upper part of the pipe is shown in Figure 7 (b).

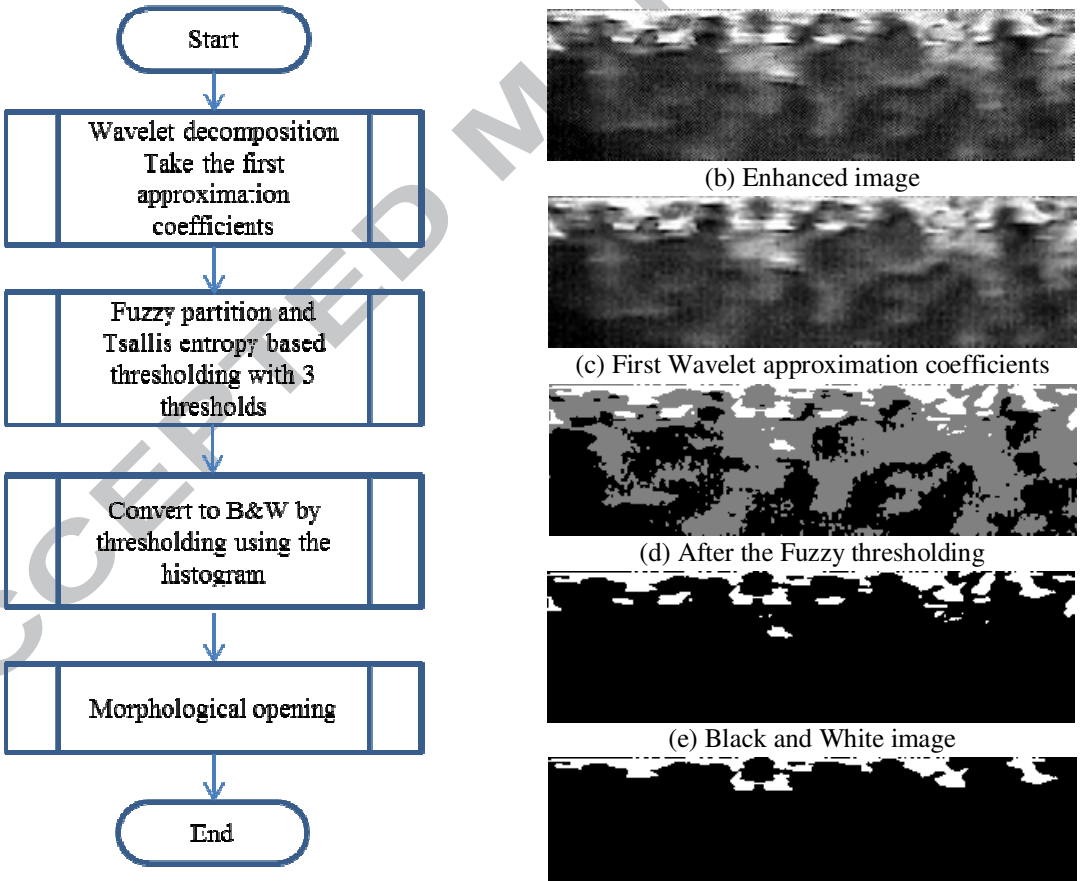

Figure 7. Segmentation using the proposed combined algorithm for an instantaneous image for the flow conditions: U_{ws}=3.0 m/s and U_{os}=1.2 m/s: (a) Flowchart of combined segmentation algorithm; (b) Enhanced

image; (c) Image of first wavelet approximation coefficients; (d) Image after Fuzzy thresholding ; (e) Image in black and white; (f) Segmented image.

3.3 Film Thickness estimation

The segmented images are calibrated to establish the relationship between pixel and length magnitudes, i.e., to determine what a pixel represents in terms of size or distance. The calibration was made using the square pattern length shown in Figure 2c. The pixel scale factor (PSF) obtained was 0.06 mm/pixel near to the pipe wall and 0.05 mm/pixel near to the pipe center.

Figure 8 shows an example of a segmented image where black represents oil and white represents water. Considering the flow lateral projection, the rows are in the horizontal direction (each row has its own pixel scale factor - PSF) and the columns are in the vertical direction (refer to Fig. 8). The water film thickness is estimated from a segmented image multiplying each white pixel by the corresponding PSF and adding the results in each column. Figure 9 is the magnification of a small portion of the image. The value in millimeters of the pixel of each row is showed at the right side and the sum result for each column is showed at the bottom. For instance, there are two pixels segmented as water in Column 2. The value in mm of the pixels is 0.06 mm, for both rows (Row 1 and Row 2). Thus, the sum for that column, i.e., the local water film thickness is equal to 0.12 mm.

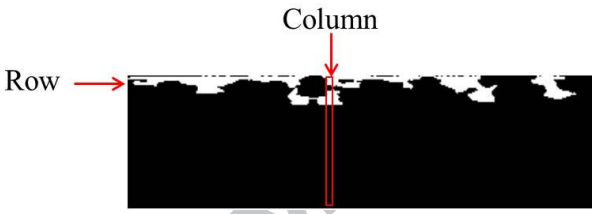

Figure 8. Segmented image for the flow conditions: U_{ws}=3.0 m/s and U_{os}=1.2 m/s.

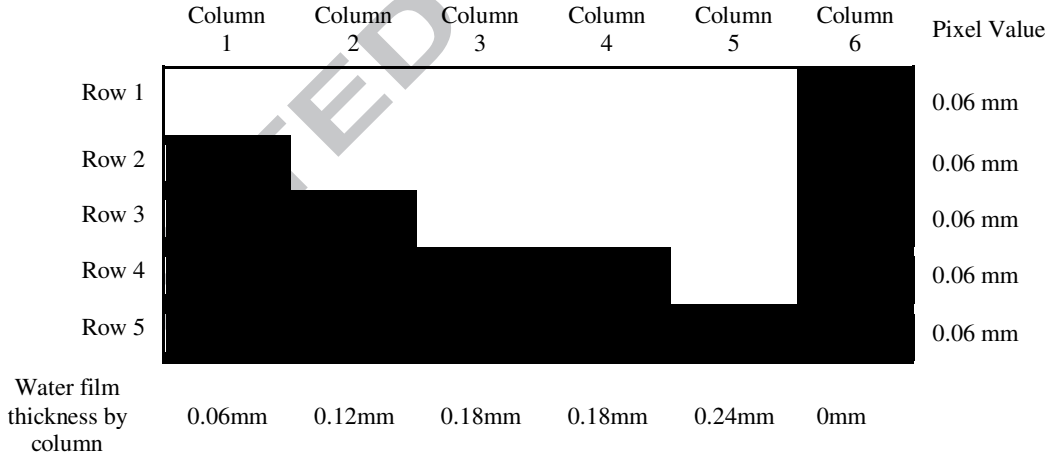

Figure 9. Illustration of estimation of water film thickness.

The averaged water-film thickness (δ) is determined as:

$$\delta = \frac{1}{N_{frames}} \sum_{frame=1}^{N_{frames}} \left(\frac{1}{N_{columns}} \sum_{Column=1}^{N_{columns}} F_{Column} \right)_{frame}, \qquad (3)$$

where N_{frames} is the total number of frames collected for each experiment (10,000 frames, in this case), $N_{columns}$ is the number the columns in one frame, and $F_{columns}$ is the water film thickness measured in each column of the image.

4 RESULTS AND DISCUSSION

4.1 Image pre-processing

In the pre-processing step each image corresponding to each experimental point was improved using the proposed algorithm. A total of 120,000 images were processed. As an example, the result of pre-processing in a single frame is represented in Figure 10 for the flow condition U_{ws}=2.5 m/s and U_{os}=1.2 m/s. Every step provides a certain degree of advantage to the process, the wavelet denoising reduces the noise, but preserves the edges (Figure 10b), the Unsharp filtering helps to emphasize texture (Figure 10c) and detail in the images and contrast enhancement improves the image contrast (Figure 10d). The proposed method produces better results than the independent methods applied alone.

4.2 Segmentation

Some frames were segmented manually and these images were compared with the automatic segmented images provided by different methods: morphology, thresholding (Otsu, ISODATA, Fuzzy), Wavelet (with K-Means and C-Means) and the proposed combined method. The manual segmentation was accomplished by using graphics editor software's. Hence, a manually segmented frame (I_m) of each experiment is used as reference and compared with the image obtained from each automatic segmentation method (I_a). Both segmented images (manual and automatic) are binary, where oil is represented by value 0 and water by value 1. TABLE II presents the parameters used to compare the segmentation methods in this work [33]. The results can be seen in Figure 11.

TABLE II. Selected parameters used to compare the segmentation methods.

Parameter	Definition	Equation	Image segmentation better if
Dice coefficient (Dice)	Measures the spatial overlap between two binary images. 0% (no overlap) and 100% (perfect agreement)	$D = \frac{2(I_a \cap I_m)}{I_a + I_m} \times 100\%$	High value
Jaccard coefficient (Jaccard)	Measures the spatial overlap between two binary images. 0% (no overlap) and 100% (perfect agreement)	$J = \frac{I_a \cap I_m}{I_a \cup I_m} \times 100\%$	High value
False Positive Dice (FPD)	Measures over-segmentation	$FDP = \frac{2(I_a \cap \bar{I}_m)}{I_a + I_m} \times 100\%$	Low value
False Negative Dice (FND)	Measures under-segmentation	$FND = \frac{2(\bar{I}_a \cap I_m)}{I_a + I_m} \times 100\%$	Low value
Number of Sites of Disagreement (NSD)	Percentage of different pixels within the manually segmented image and the automatic method.	$NSD = \frac{1}{NM}\left(\sum_{0}^{N-1}\sum_{0}^{M-1}\lvert I_a - I_m\rvert\right) * 100\%$	Low value

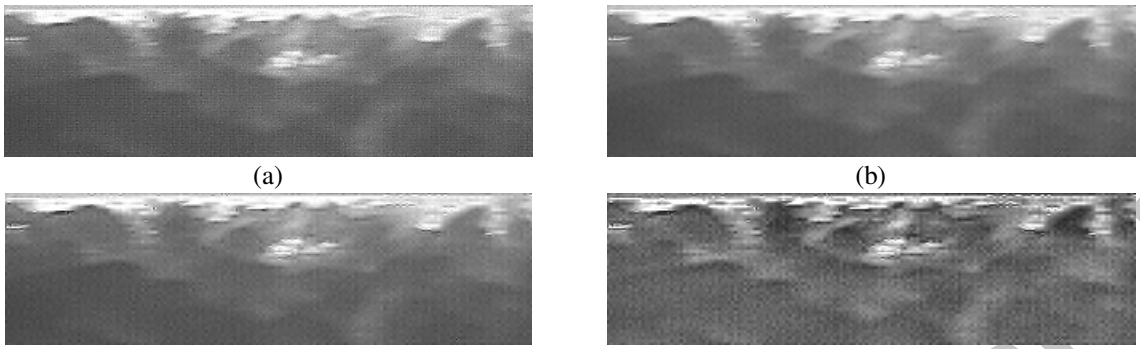

Figure 10. Results visual enhancement of image provided by the proposed pre-processing algorithm for a snapshot at flow condition U_{ws}=2.5 m/s and U_{os}=1.2 m/s: (a) original image; b) image after wavelet denoising; (c) denoised image after unsharp filtering; and (d) unsharped image after contrast improvement with CLAHE with Raylegh distribution.

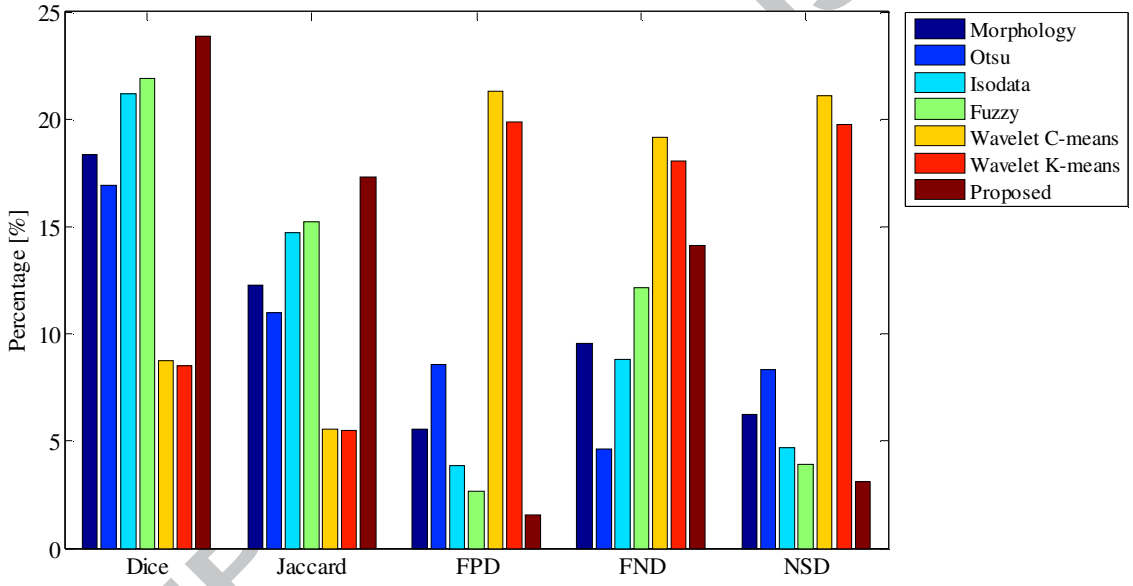

Figure 11. Mean of parameters used to compare the segmentation algorithms

In accordance to the value of the parameters (quality metrics) and through visual inspection it was possible to conclude that the proposed combined method presented the best results for the segmentation of the dispersed oil-water flow images (Figure 11). Particularly, the Dice and Jaccard parameters are higher, and FDP and NDS present lower values, which indicates that the performance of the proposed segmentation algorithm is better in comparison to the other methods. One can see in Figure 12 the segmented images obtained by applying the different segmentation methods and the proposed combined method. Figure 12 corresponds to the flow condition U_{ws}=3.0 m/s and U_{os}= 1.2 m/s and top side of the pipe.

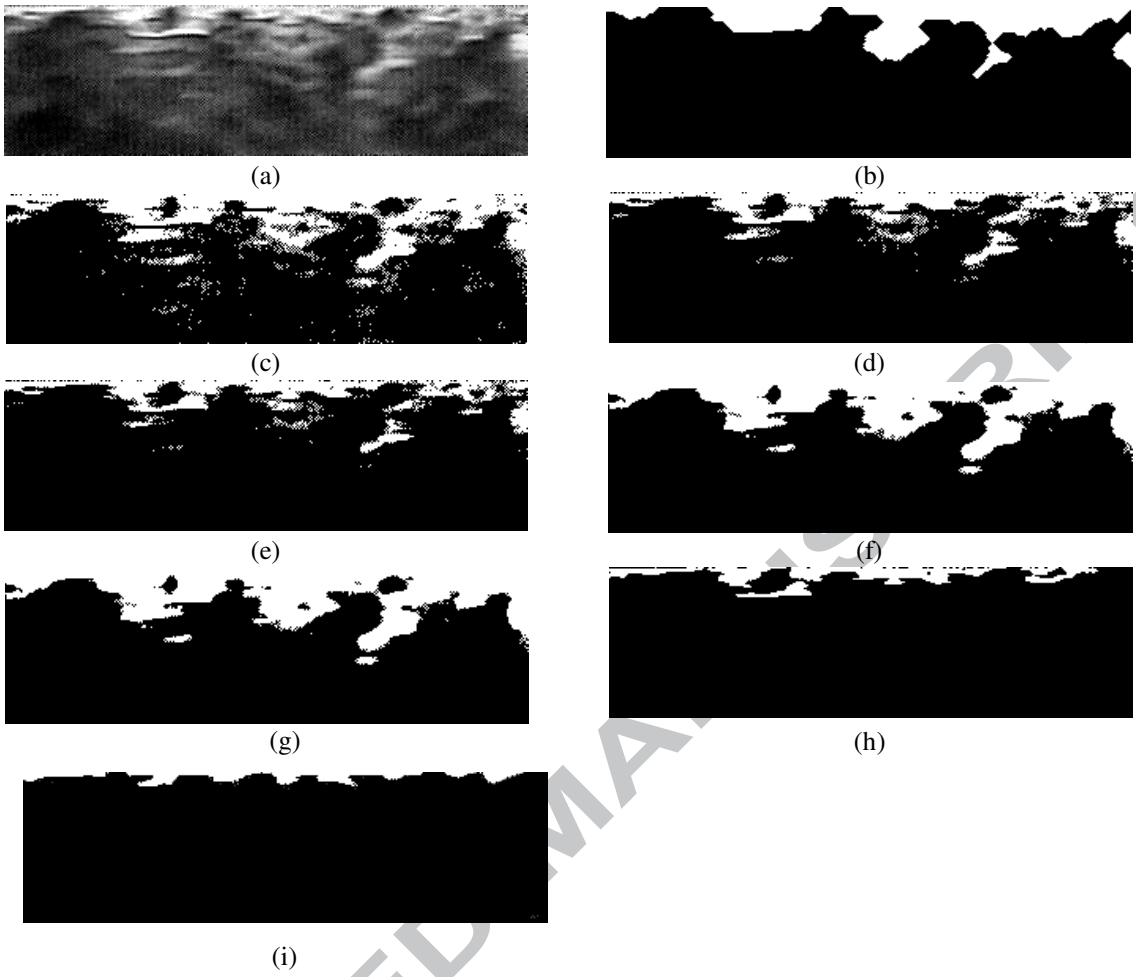

Figure 12. Segmentation results obtained from different methods for a snapshot and flow condition U_{ws}=3.0 m/s and U_{os}= 1.2 m/s: (a) enhanced image; (b) segmented using morphology; (c) segmented by Otsu thresholding; (d) segmented by ISODATA thresholding; (e) segmented by fuzzy thresholding; (f) segmented using wavelet and K-Means; (g) segmented using wavelet and C-Means; (h) segmented using combined method; (i) manually segmented

In general, the combined method was able to find the interface between water and oil. The other methods strongly overestimate the water area.

4.3 Film thickness estimation and comparison with a model from the literature

One can see in TABLE III the values of film thickness obtained by the combined segmentation method described in Section 3.3 for mixture velocities (U_m) varying from 3.1 to 4.2 m/s and input oil fractions (C_o) from 14% to 43%. For these flow conditions it was observed a dispersed flow pattern which is characterized by oil droplets uniformly dispersed throughout the continuous water phase. However, a thin water film can be noticed near the pipe wall, i.e., near the top and bottom of the pipe.

The water film at the bottom of the pipe was in general thicker than that measured at the upper part of the tube, which is expected because of the density difference between the fluids (oil and water) and the effect of gravity. However, it is possible to observe in Figure 13 that with increasing the mixture velocity the film thickness decreases, especially at the bottom of the pipe. The thicknesses measured at the top and bottom of the pipe become closer, indicating a possible formation of a more axisymmetric flow.

TABLE III. Film thickness estimated at the top and bottom of the pipe for different flow conditions.

Exp	C_o [-]	U_m [m/s]	δ_{top} [mm]	δ_{bottom} [mm]
1	0.14	3.5	0.42	2.30
2	0.19	3.7	0.37	1.68
3	0.19	3.1	0.48	2.57
4	0.21	3.8	0.31	1.11
5	0.24	3.3	0.39	2.10
6	0.25	4.0	0.35	0.78
7	0.26	3.4	0.34	1.38
8	0.29	4.2	0.30	0.66
9	0.29	3.5	0.43	1.25
10	0.32	3.7	0.37	0.96
11	0.38	3.2	0.58	1.31
12	0.43	3.5	0.34	0.38

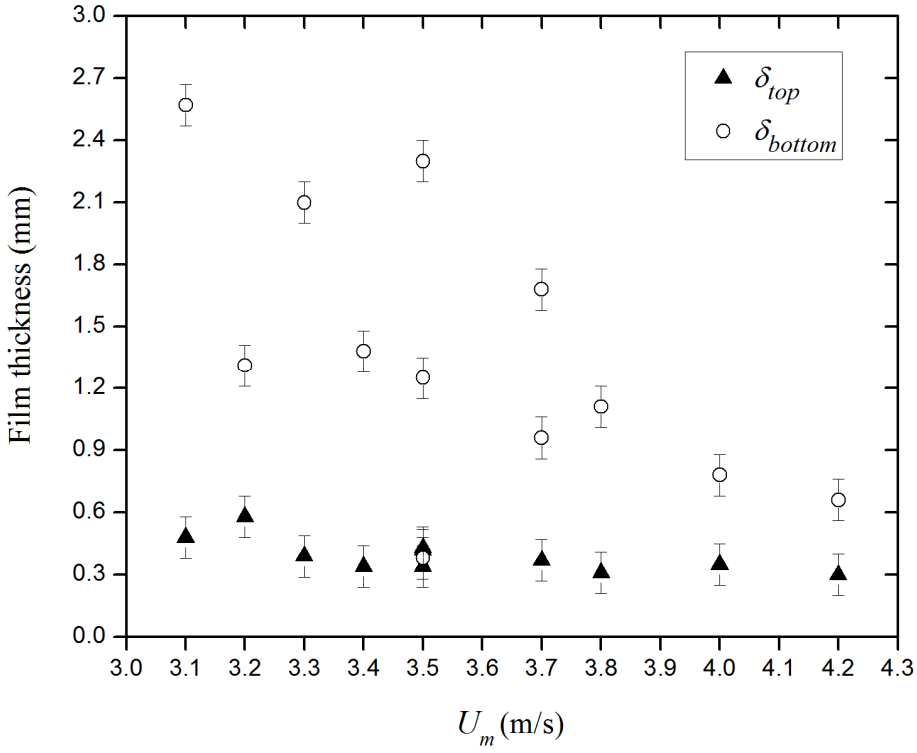

Figure 13. Comparison between the film thicknesses measured at the top and bottom of the pipe using the purposed algorithm for each experiment.

A phenomenological model has been developed by Rodriguez et al. [6] and [34] to predict the water film thickness in dispersed oil-in-water flow. The model is based on the assumption of existence of a thin laminar water film flowing adjacent to the pipe wall and surrounding a turbulent core of oil-water dispersion. It uses pressure-drop, holdup data and physical properties of the fluids to estimate the film thickness.

One can see in Figure 14 a comparison between the film thickness estimated by the proposed visual technique (top side of the pipe) and the film thickness predicted by the model of Rodriguez et

al. [6] and [34]. The model underestimates the experimental value with an average relative error (ARE) of 34%. On the other hand, if one considers the uncertainty of the proposed experimental technique, the agreement between data and prediction is quite fair. In addition, the model correctly captures the observed trend, i.e., a reduction in the film thickness with increasing the mixture velocity.

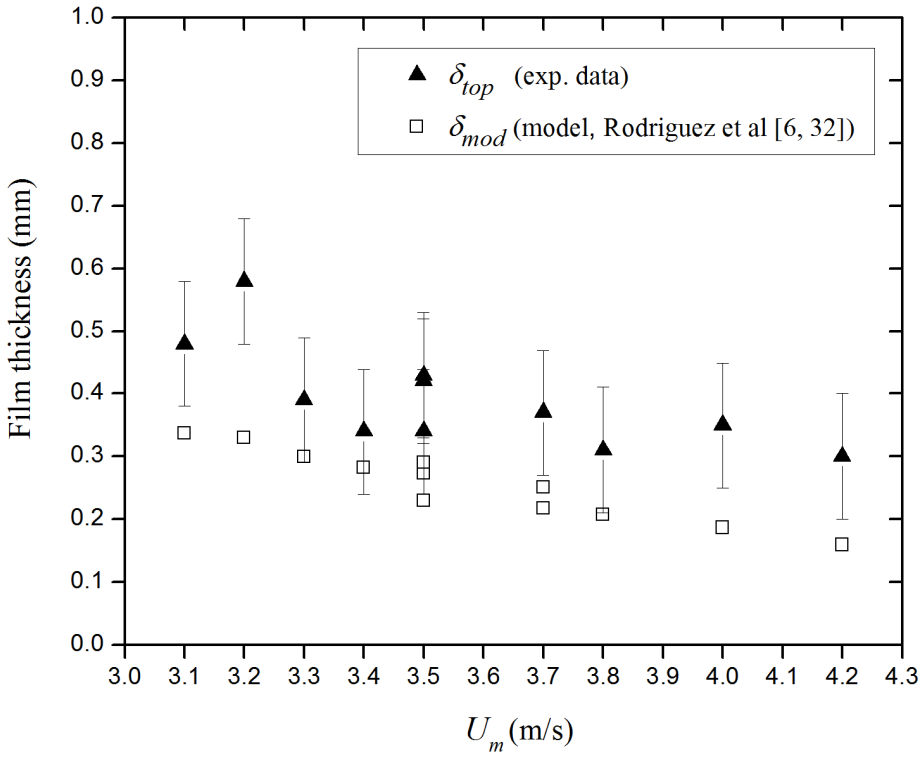

Figure 14. Comparison between the film thickness predicted by Rodriguez et al. model [6][34] and the one measured using the image processing technique.

The following average relative error (*ARE*) is considered in this work:

$$ARE = 100 \frac{\sum_{1}^{N} \sqrt{\left(\frac{\delta_{mod} - \delta_{top}}{\delta_{top}} \right)^2}}{N} [\%], \qquad (4)$$

where δ_{mod} and δ_{top} refer to film thickness predicted by the model (Rodriguez et al. [6] and [34]) and that estimated by image processing using the proposed algorithm, respectively. *N* is the number of experimental points.

5 CONCLUSIONS

A visual technique has been applied for near-wall flow measurements in order to detect the presence of a liquid film in highly dispersed flow of viscous oil in water in a horizontal acrylic pipe. An experimental setup was assembled for image acquisition. A digital image processing was applied to estimate the water film thickness. The measurements of the film thickness were performed on image snapshots and then averaged. The film thickness obtained by digital image processing was compared to predictions of a model from the literature.

Different methods were implemented for the pre-processing and segmentation of the flow images. The methods were compared with results of a manual segmentation technique by using some metrics found in the literature. A combined method is being proposed for image processing of the typical two-phase flow under study in this work, which is based on the systematic combination of different methods for pre-processing and segmentation of the images. The pre-processing comprises Wavelet denoising, Unsharp filtering and contrast enhancement. The proposed methodology for segmentation is a combination of the following methods: wavelet decomposition, fuzzy partition and Tsallis entropy based thresholding, with three thresholds conversion to binary using the histogram, and morphological opening. The combined method performed significantly better when compared to the results obtained with traditional techniques applied individually.

A water film with a maximum thickness of 0.58 mm was measured at the upper part of the pipe at highly dispersed viscous oil-water flow. The detection of this thin water film adjacent to the pipe wall in the flow of oil-in-water dispersions can contribute to the study of the drag reduction phenomenon observed in this type of two-phase flow pattern.

ACKNOWLEDGEMENTS

The authors are grateful to FAPESP (Fundação de Amparo à Pesquisa do Estado de São Paulo, proc. 2010/08688-3), CAPES (Coordenação de Aperfeiçoamento de Pessoal de Nível Superior) and CNPq (Conselho Nacional de Desenvolvimento Científico e Tecnológico). The authors are also grateful to Hélio Trebi for his support and contribution in part of the experimental work.

BIBLIOGRAPHY

[1] R. Pal, "Mechanism of Turbulent Drag Reduction in Emulsions and Bubbly Suspensions," *Ind. Eng. Chem. Res.*, vol. 46, pp. 618–622, 2007.

[2] A. Omer and R. Pal, "Pipeline Flow Behavior of Water-in-Oil Emulsions with and without a Polymeric Additive in the Aqueous Phase," *Chem. Eng. Technol.*, vol. 33, no. 6, pp. 983–992, Jun. 2010.

[3] P. Angeli and G. F. Hewitt, "Pressure gradient in horizontal liquid-liquid flows," *Int. J. Multiph. Flow*, vol. 24, no. 7, pp. 1183–1203, 1998.

[4] J. Lovick and P. Angeli, "Experimental studies on the dual continuous flow pattern in oil–water flows," *Int. J. Multiph. Flow*, vol. 30, no. 2, pp. 139–157, Feb. 2004.

[5] K. Ioannou, O. J. Nydal, and P. Angeli, "Phase inversion in dispersed liquid–liquid flows," *Exp. Therm. Fluid Sci.*, vol. 29, no. 3, pp. 331–339, Mar. 2005.

[6] I. H. Rodriguez, H. K. B. Yamaguti, M. S. De Castro, M. J. Da Silva, and O. M. H. Rodriguez, "Drag Reduction Phenomenon in Viscous Oil-Water Dispersed Pipe Flow : Experimental Investigation and Phenomenological Modeling," *AIChE J.*, vol. 58, no. 9, pp. 2900–2910, 2012.

[7] W. W. Clark, "Liquid Film Thickness Measurement," *Multiph. Sci. Technol.*, vol. 14, no. 1, pp. 1–74, 2002.

[8] C. B. Tibiriçá, F. J. do Nascimento, and G. Ribatski, "Film thickness measurement techniques applied to micro-scale two-phase flow systems," *Exp. Therm. Fluid Sci.*, vol. 34, no. 4, pp. 463–473, May 2010.

[9] R. V. A. Oliemans, G. Ooms, H. L. Wu, and A. Duijvestijn, "Core-Annular Oil/Water flow: Turbulent -Lubricanting-Film Model and Measurement in a 5cm Pipe Loop," *Int. J. Multiph. Flow*, vol. 13, no. 1, pp. 23–31, 1987.

[10] S. Thiele, M. J. Da Silva, and U. Hampel, "Capacitance Planar Array Sensor for Fast Multiphase Flow Imaging," *IEEE Sens. J.*, vol. 9, no. 5, pp. 533–540, May 2009.

[11] M. J. Da Silva, E. Schleicher, and U. Hampel, "Capacitance wire-mesh sensor for fast measurement of phase fraction distributions," *Meas. Sci. Technol.*, vol. 18, no. 7, pp. 2245–2251, Jul. 2007.

[12] J. M. Lopez, R. Mohan, O. Shoham, S. Wang, and G. Kouba, "Experimental Investigation of Falling Liquid Film in Vertical Downward Two-Phase Pipe Flow," in *ASME 2012 Fluids Engineering Division Summer Meeting Volume 2: Fora*, 2012, pp. 99–109.

[13] P. Angeli and G. . Hewitt, "Flow structure in horizontal oil–water flow," *Int. J. Multiph. Flow*, vol. 26, no. 7, pp. 1117–1140, 2000.

[14] A. Bonilla Riaño, A. C. Bannwart, and O. M. H. Rodriguez, "Film thickness planar sensor in oil-water flow: prospective study," *Sens. Rev.*, vol. 35, no. 2, pp. 200–209, Mar. 2015.

[15] B. J. Witt, H. Coronado-Diaz, and R. J. Hugo, "Optical contouring of an acrylic surface for non-intrusive diagnostics in pipe-flow investigations," *Exp. Fluids*, vol. 45, no. 1, pp. 95–109, Feb. 2008.

[16] M. L. Lowe and P. H. Kutt, "Refraction through cylindrical tubes," *Exp. Fluids*, vol. 320, no. 13, pp. 315–320, 1992.

[17] T. L. Narrow, M. Yoda, and S. I. Abdel-Khalik, "A simple model for the refractive index of sodium iodide aqueous solutions," *Exp. Fluids*, vol. 28, no. 3, pp. 282–283, Mar. 2000.

[18] R. Budwig, "Refractive index matching methods for liquid flow investigations," *Exp. Fluids*, vol. 17, no. 5, pp. 350–355, Sep. 1994.

[19] A. Bonilla Riaño, A. C. Bannwart, and O. M. H. Rodriguez, "Holdup Estimation in Core Flow Using Image Processing," in *Instrumentation and Measurement Technology Conference (I2MTC), 2013 IEEE International*, 2013, pp. 1–5.

[20] A. Bonilla Riaño and O. M. H. Rodriguez, "Improvement of Dispersed Oil-Water Pipe Flow Images," in *Multiphase Flow Journeys-JEM 2015*, 2015.

[21] E. Juliastuti and L. Epsilawati, "Image contrast enhancement for film-based dental panoramic radiography," in *2012 International Conference on System Engineering and Technology (ICSET)*, 2012, no. 1, pp. 1–5.

[22] S. Arivazhagan, S. Deivalakshmi, and K. Kannan, "Performance Analysis of Image Denoising System for different levels of Wavelet decomposition," *Int. J. Imaging Sci. Eng.*, vol. 1, no. 3, pp. 104–107, 2007.

[23] R. C. Gonzales and R. E. Woods, *Digital Image Processing*, Second edi. Prentice Hall, 2002.

[24] R. C. Gonzalez and A. Perez, "An Iterative Thresholding Algorithm for Image Segmentation," *IEEE Trans. Pattern Anal. Mach. Intell.*, vol. PAMI-9, no. 6, pp. 742–751, 1987.

[25] N. Otsu, "A Threshold Selection Method from Gray-Level Histograms," *IEEE Trans. Syst. Man. Cybern.*, vol. SMC-9, no. 1, pp. 62–66, 1979.

[26] C. H. Bindu, "An improved medical image segmentation algorithm using otsu method," *Int. J. Recent Trends Eng.*, vol. 2, no. 3, pp. 88–90, 2009.

[27] F. Dias, "Thresholding using the ISODATA Clustering Algorithm," *IEEE Trans. Syst. Man. Cybern.*, vol. SMC-10, no. 11, pp. 771–774, 1980.

[28] A. El-Zaart, "Images thresholding using ISODATA technique with gamma distribution," *Pattern Recognit. Image Anal.*, vol. 20, no. 1, pp. 29–41, Apr. 2010.

[29] S. Sarkar and S. Das, "Multilevel Image Thresholding Based on 2D Histogram and Maximum Tsallis Entropy— A Differential Evolution Approach," *IEEE Trans. Image Process.*, vol. 22, no. 12, pp. 4788–4797, Dec. 2013.

[30] R. M. Haralick, S. R. Sternberg, and X. Zhuang, "Image Analysis using Mathematical Morphology," *IEEE Trans. Pattern Anal. Mach. Intell.*, vol. PAMI-9, no. 4, pp. 532–550, 1987.

[31] M. N. Kurnaz, Z. Dokur, and T. Olmez, "Segmentation of ultrasound images by using wavelet transform," *Proc. 25th Annu. Int. Conf. IEEE Eng. Med. Biol. Soc. (IEEE Cat. No.03CH37439)*, no. i, pp. 657–659, 2003.

[32] T. Kanungo, D. M. Mount, N. S. Netanyahu, C. D. Piatko, R. Silverman, and a. Y. Wu, "An efficient k-means clustering algorithm: analysis and implementation," *IEEE Trans. Pattern Anal. Mach. Intell.*, vol. 24, no. 7, pp. 881–892, Jul. 2002.

[33] N. E. Jacob and M. V. Wyawahare, "Tibia Bone Segmentation in X-ray Images - A Comparative Analysis," *Int. J. Comput. Appl.*, vol. 76, no. 9, pp. 34–41, 2013.

[34] I. H. Rodriguez, "Experimental study and modeling of flow of inverse emulsion in pipes," University of Sao Paulo, 2014.

Highlights

- Film thickness measurements using high speed camera
- Experimental study of flow near the pipe wall in highly dispersed oil-water flow
- Application of digital image processing techniques to quantify the film thickness near the wall
- New image processing methodology for highly dispersed oil-water flow images
- Comparisons of the proposed methodology with a phenomenological model and gold standard images